

Chemical Science



Accepted Manuscript

This article can be cited before page numbers have been issued, to do this please use: S. Su and Q. Miao, *Chem. Sci.*, 2025, DOI: 10.1039/D5SC06726J.



This is an Accepted Manuscript, which has been through the Royal Society of Chemistry peer review process and has been accepted for publication.

Accepted Manuscripts are published online shortly after acceptance, before technical editing, formatting and proof reading. Using this free service, authors can make their results available to the community, in citable form, before we publish the edited article. We will replace this Accepted Manuscript with the edited and formatted Advance Article as soon as it is available.

You can find more information about Accepted Manuscripts in the <u>Information for Authors</u>.

Please note that technical editing may introduce minor changes to the text and/or graphics, which may alter content. The journal's standard <u>Terms & Conditions</u> and the <u>Ethical guidelines</u> still apply. In no event shall the Royal Society of Chemistry be held responsible for any errors or omissions in this Accepted Manuscript or any consequences arising from the use of any information it contains.



View Article Online DOI: 10.1039/D5SC06726J

Robust π-Conjugated Radical Cations

Shilong Sua, Qian Miao*, a, b

Received 00th January 20xx, Accepted 00th January 20xx

DOI: 10.1039/x0xx00000x

 π -Conjugated radical cations, open-shell species carrying a positive charge, serve as charge carriers in p-type organic semiconductors, underpinning the operation of various organic electronic devices. Although they are traditionally perceived as highly reactive and challenging to isolate under ambient conditions, recent advances in electronic and steric stabilization have enabled the isolation and full characterization of a number of robust π -conjugated radical cations. This review provides a comprehensive overview of fully characterized π -conjugated radical cations, with particular emphasis on species identified via single-crystal X-ray crystallography within the last two decades. We highlight structural features and stabilization strategies that enable ambient stability, and explore structure–property relationships critical to their application in organic electronic materials, indicating the potential to enhance material stability and improve device performance. Based on this analysis, we assess the current state of the field and outline promising future directions.

1. Introduction

This article is licensed under a Creative Commons Attribution-NonCommercial 3.0 Unported Licence

Open Access Article. Published on 19 2025. Downloaded on 20/11/25 23:15:55

π-Conjugated radical cations are open-shell species that carry either a positive charge, typically generated by oxidation of a neutral, closed-shell π -conjugated system.¹ They play a central role in organic electronic materials and devices because the doped states of p-type organic semiconductors are commonly associated with radical cations. ² As a result, most organic conductors rely on π -conjugated radical cation salts, and the operation of various organic electronic devices depends on the controlled generation of π -conjugated radical cations. This is well illustrated by early examples of conducting radical cation salts, as shown in Fig. 1. Oxidation of tetrathiafulvalene (TTF) with Cl2 results in the radical cation salt TTF*+Cl-,3 which exhibits a room-temperature conductivity of 0.27 ± 0.1 S cm⁻¹ in microcrystalline form.⁴ Similarly, electrochemical oxidation of bis(ethylenedithiolo)tetrathiafulvalene (BEDT-TTF) in the presence of CuSCN produces the crystal of (BEDT-TTF)2*+Cu(SCN)2-, in which two BEDT-TTF molecules dimerize through short S···S contacts and share a single unpaired electron. The resulting single crystal displays a roomtemperature conductivity of 14 S cm⁻¹ and becomes a superconductor at 10.4 K under ambient pressure. 5 The third the perchlorate of example the tetrakis(methylthio)pyrene (TMTP) radical cation. (TMTP)2*+ClO4-, which exhibits an exceptionally high roomtemperature conductivity in the range of 156 to 667 S cm⁻¹.6, 7 Consistent with this behavior, the neutral TMTP molecule functions as an organic semiconductor, recently reported to exhibit a remarkably high hole mobility of 32 cm² V⁻¹ s⁻¹ in single-crystal organic field-effect transistors (OFETs). ⁸

$$\begin{array}{c|c} S & S \\ \downarrow & \downarrow \\ TTF^{+}CI^{-} \\ \\ \hline \\ S & S & S \\ \hline \\ S & S & S \\ \hline \\ S & S & S \\ \hline \\ Cu(SCN)_{2}^{-} \\ \hline \\ (BEDT-TTF)_{2}^{+}Cu(SCN)_{2}^{-} \\ \end{array}$$

$$(TMTP)_{2}^{+}CIO_{4}^{-}$$

Fig.1 Early examples of organic conductors and superconductors based on radical cation salts.

The unique electronic structures of π -conjugated radical cations—combining both radical and ionic characteristics give rise not only to electrical conductivity 9 but also to magnetic 10 and optical properties 11, 12 due to their unpaired spin densities. These features open avenues unconventional applications, 13, 14, 15, 16 such as doublet emission in organic light-emitting diodes (OLEDs) with 100% internal quantum efficiency. 17 Despite their importance, π conjugated radical cations typically exhibit high reactivity, which often results in difficulties in isolating them in pure form and limits their detailed structural and spectroscopic characterization. Furthermore, their paramagnetic nature renders NMR signals undetectable. Consequently, full characterization of these species typically requires singlecrystal X-ray crystallography. Over the past two decades, advances in electronic and steric stabilization have enabled the isolation of a number of ambient-stable π -conjugated radical cations. This review highlights these advances and shows how the full characterization of these stable systems has revealed key structural motifs governing stability. These

^a Department of Chemistry, The Chinese University of Hong Kong, Shatin, New Territories, Hong Kong, China. E-mail: miaoqian@cuhk.edu.hk

b. State Key Laboratory of Synthetic Chemistry, The Chinese University of Hong Kong, Shatin, New Territories, Hong Kong, China

ARTICLE Journal Name

insights are crucial for the rational design of more robust, high-performance organic electronic materials.

While recent reviews have separately covered organic radicals and organic ions, they have not comprehensively addressed π -conjugated radical cations. Reviews on π conjugated radicals have predominantly focused on neutral species, ^{13, 14, 18, 19, 20, 21} while those on hydrocarbon-based cations have overlooked their radical character. ²² This review fills this gap by providing a comprehensive overview of fully characterized π -conjugated radical cations, with a particular emphasis on structures resolved by single-crystal X-ray crystallography. We examine key structural motifs that impart stability and highlight their applications in organic electronics. Finally, we assess the current state of the field and suggest future research directions. To systematically organize this body of work, we classify the discussed radical cations into three categories. Mono-radical cations refer to species containing a single unpaired electron and a single positive charge. Multiple radical cations are those that possess more than one unpaired electron and/or carry more than a single positive charge. Fractional radical cations describe systems in which the unpaired electrons and/or positive charges are shared by multiple π -conjugated molecules, resulting in a non-integer (fractional) distribution of spin or charge per molecule. In each category, π -conjugated radical cations are grouped according to the stabilization strategies employed.

2. Mono-radical cations

This article is licensed under a Creative Commons Attribution-NonCommercial 3.0 Unported Licence

Open Access Article. Published on 19 2025. Downloaded on 20/11/25 23:15:55.

This section classifies mono-radical cations into three groups based on their structural features. When a mono-radical cation exhibits more than one such feature—for example, containing both a nitrogen and a sulfur atom—the structural element that contributes more significantly to the stabilization of the radical cation takes precedence in classification. Only in rare cases are radical cations with different structural features discussed together, as their conjugated backbones are closely related.

2.1 Conjugated hydrocarbons

Radical cations of conjugated hydrocarbons are usually stabilized by two strategies: steric protection delocalization of spin density and charge. Steric protection involves introducing bulky substituents to kinetically protect the radical cation from dimerization or nucleophilic attacks, albeit at the cost of hindering or even blocking π - π interactions. Bulky groups employed in the reported radical cations of polycyclic arenes include tert-butyl and mesityl groups as well bicyclo[2.2.2]octene and norbornene units, demonstrated with Fig. 2. Hexa-peri-hexabenzocoronene (HBC) and quaterphenyl represent fragments of graphene and polyp-phenylene, respectively, and compounds 1 and 2 are their tert-butylated derivatives, respectively. Chemical oxidation of 1 with $Ag^{+}(Al(OC(CF_3)_3)_4)^{-}$ affords its radical cation, which forms a π -stacked dimer exhibiting short C···C distances ranging from 3.3 to 3.5 Å in the crystal of $1^{-+}(AI(OC(CF_3)_3)_4)^{--}$. In comparison, electrochemical oxidation of 1 in the presence of tetrabutylammonium hexafluoroarsenate at -30 °C results

in the crystal of $(1)_2^{\bullet+} \text{AsF}_6^-$, where two molecules of 1 formal π -stacked dimer. ²⁴ Averagely, each molecule of 1 possesses half a radical and half a positive charge although bond length analysis of the crystal structure shows the two molecules in the dimer are different, suggesting the radical and positive charge are not evenly distributed among them. Oxidation of compound 1 with nitrosonium hexachloroantimonate $(NO^+SbCl_6^-)$ under an argon atmosphere at 10° C results in 10° It crystallizes from solution at 10° C as 10° Notably, in the above radical cation salts, the 10° solvent molecules without further 10° interactions possibly due to steric hindrance of the bulky substituents.

Fig.2 Sterically protected conjugated hydrocarbons whose radical cations were fully characterized.

The radical cations of compounds 3 26 and 4 27 are sterically shielded by bulky substituents: mesityl and 2,6-dimethyl-4tert-butylphenyl groups, respectively. Notably. substituents are strategically positioned on carbon atoms with the highest spin density, ensuring efficient protection of the radical centre. For dibenzoperopyrene 3, the radical cation is further stabilized through delocalization of both positive charge and unpaired spin across the polycyclic framework. This stabilization is enhanced by global aromaticity, as evidenced by diatropic ring currents observed along the edges of the polycyclic system in the anisotropy of the induced current density (ACID) plot. As a result, the radical cation salt 3°+SbCl₆exhibits high air stability in the solid state, remaining intact for at least two weeks without significant degradation. Compound 4 similarly benefits from delocalization of its unpaired spin and positive charge. Structural analysis comparing the neutral and

Journal Name ARTICLE

radical cation forms of **4** in the crystal reveals that the external naphthalene units undergo notable changes in bond lengths due to charge redistribution.

In 1993, Komatsu et al. demonstrated that the radical cation of cyclooctatetraene could be kinetically stabilized in its sterically congested derivative 5a (Fig. 2), which features four fused bicyclo[2.2.2]octene units. 28 The single crystal of 5a*+SbCl6- remains stable for several hours under ambient conditions and can be stored under refrigeration for months without decomposition. Employing the same steric protection strategy, Komatsu et al. later synthesized bicyclo[2.2.2]octene-fused derivatives of naphthalene (5b in Fig. 2), biphenylene (5c in Fig. 2) and anthracene. These radical cations were crystallized as hexachloroantimonate salts, which are persistent at ambient temperature even in air. Notably, crystal structural analysis of 5c reveals that oxidation of biphenylene to its radical cation form leads to a significant shortening (by 0.042 Å) of the bonds connecting the two benzene rings, consistent with the reduction of destabilizing 4π antiaromaticity in the neutral state. Similarly, Kochi et al. reported compound 6, a naphthalene derivative sterically shielded by fusing with tetramethylcyclohexane moieties.²⁹ The corresponding radical cation, 6°+, was isolated as 6°+SbCl₆crystals. Interestingly, cocrystallization of 6°+SbCl₆- with unsubstituted naphthalene (naph) in CH2Cl2 solution afforded dark-green crystals of (6°+)2(naph)(SbCl₆-)2, which are stable in air at room temperature for several days. In this crystal, two 6°+ cations sandwich a neutral naphthalene molecule, forming a diradical dicationic (hetero)trimer in which the central naphthalene is rotated by 90° relative to the radical cations. Bond length analysis suggests that negative charge is transferred from naphthalene to 6°+, which in turn is not a true mono radical cation. Likewise, Ishihara et al. used norbornene units to sterically protect the radical cation of pdimethoxybenzene in compound 7.30 Oxidation of 7 by FeCl₃ produces a persistent radical cation, which crystallizes as 7°+FeCl₄-. This result confirms that single-electron oxidation of arenes to yield radical cations is achievable under typical Scholl reaction conditions, providing evidence to support the radical cation mechanism.31

The unpaired spin and positive charge in radical cations of conjugated hydrocarbons can be effectively delocalized by π systems such as phenalenyl, Thiele's hydrocarbon, and azulene. As shown in Fig. 3a, phenalenyl delocalizes a radical or a positive charge across seven carbon atoms via resonance. Leveraging this capability, Kubo et al. designed and synthesized acetylene-linked bisphenalenyl **8**,³² resonates with a closed-shell cumulene structure (Fig. 3b). Compound 8 exhibits biradical character, confirmed experimentally and theoretically. It reacts with 2,3,5,6tetrafluoro-tetracyanoquinodimethane (F4-TCNQ) to form a charge-transfer complex, 8°+(F₄-TCNQ)-, with complete charge transfer, as determined by Raman spectroscopy. This crystal remains stable in ambient conditions for weeks and shows a conductivity of 1.43 S cm⁻¹ at 280 K owning to efficient π - π overlap in a π -stacked one-dimensional chain with a staggered packing motif. Notably, cooling 8°+(F₄-TCNQ)- to 90 K induces

formation of a C–C σ bond between a F₄–TCNQ's $G(N)_2$ group and a phenalenyl carbon. Unlike **8**, O^{C} and O^{C} be a substituted by the O^{C} and $O^$

Fig.3 (a) Resonance structures of phenalenyl radical or cation; (b) bisphenalenyls 8–10.

As shown in Fig. 4a, the radical cation of Thiele's hydrocarbon (TH) is stabilized by the formation of a central benzene ring. Such aromaticity-enhanced stabilization has been used to develop stable conjugated radical cations based on TH (shown in blue), as demonstrated by compounds 11-13 in Fig. 4b. Bunz et al. found that the radical cations of N, N'diarylated dihydrodiazapentacene 11a/b remained stable in CH₂Cl₂ for 24 h under ambient condition. ³⁴ In the crystal structure of 11a°+SbF₆-, the centre ring and adjacent nitrogenembedded six-membered ring have less bond length alternation than the neutral form, indicating increased aromaticity in these rings, which is also supported by NICS(1)zz calculation. Such an increase in aromaticity can explain the observed high stability of the radical cation of 11a/b. For the same reason, the radical cation of compound 12 exhibits similar stability as its N-substituted analogue (11a/b). Its salt 12°+SbF₆- showed negligible spectral change after one day under aerated conditions at room temperature.35 Compound 13 is similar to 12 by containing oxygen-incorporated TH in

10°

Journal Name

This article is licensed under a Creative Commons Attribution-NonCommercial 3.0 Unported Licence.

Open Access Article. Published on 19 2025. Downloaded on 20/11/25 23:15:55.

spite of extra carbonyl groups in the π -backbone. ³⁶ The radical cation of **13** is thermodynamically stabilized by delocalizing its unpaired spin across the whole molecule including aniline nitrogen and benzoyl carbon atoms. As a result, **13**°+SbF₆⁻ is very stable in solid state with no degradation after 10 months and in CH₂Cl₂ solution with no degradation after 7 days under ambient conditions and room light. Spin-coated films of neutral **13** function as a p-type semiconductor with field-effect mobility of 1.3×10^{-5} cm² V⁻¹ s⁻¹, while spin-coated films of **13**°+DDQ⁻ exhibits ohmic behavior with a room-temperature conductivity of 7.7×10^{-3} S cm⁻¹. Having two C atoms replaced by B and N atoms, respectively, compounds **14** is a B-N analogue of TH.³⁷ Oxidation of **14** with Ag+SbF₆⁻ results in

14°+SbF₆-, which represents a rare example of an isolable

boron-containing radical cation.

Fig.4 (a) Thiele's hydrocarbon (TH) and its radical cation; (b) compounds derived from TH (11–13) and a BN analogue of TH (14).

A seven-membered carbocycle capable of forming an aromatic tropylium cation has also been employed as a structural motif to stabilize radical cations, as exemplified by compounds 15 and 16 (Fig. 5). 38 DFT calculations revealed that upon one-electron oxidation, the seven-membered ring in 15** becomes more positively charged compared to neutral 15, while the unpaired spin is delocalized across the framework, with higher density localized on the seven-membered ring and the inner rim of the five-membered rings, the latter being shielded by the helical conformation of 15°+. Stepwise chemical oxidation of 16 with NO+SbF₆- generated the radical cation (16°+) and the dication (16°+), which were isolated as their hexafluoroantimonate salts. ³⁹ DFT calculations indicate that in $\mathbf{16}^{\bullet+}$, the spin is delocalized across the π -backbone, with higher density on the seven-membered rings, while in 162+, the positive charges are predominantly located on the sevenmembered carbocycles. In the single crystal of $16^{**}Sh_{16}^{**}Sh_{16}^{**} = 16^{**}$ adopts a cisoid conformation, and pack of the order of the factorial dimer. Partial oxidation with NO+SbF₆⁻ can yield fractional radical cation salt. Interestingly, partial oxidation of 16 with NO+SbF₆⁻ resulted in crystals of a mixed-valence species $16 \cdot (16^{**})_3$ consisting of one-quarter equivalent of the neutral molecule and three-quarters equivalent of the radical cation. The crystal structure of this mixed-valence species features a huge trigonal unit cell that contains 72 molecules of 16, 54 SbF₆⁻ counter anions and 101 disordered hexane molecules.

Fig. 5 π -systems containing seven-membered carbocycles.

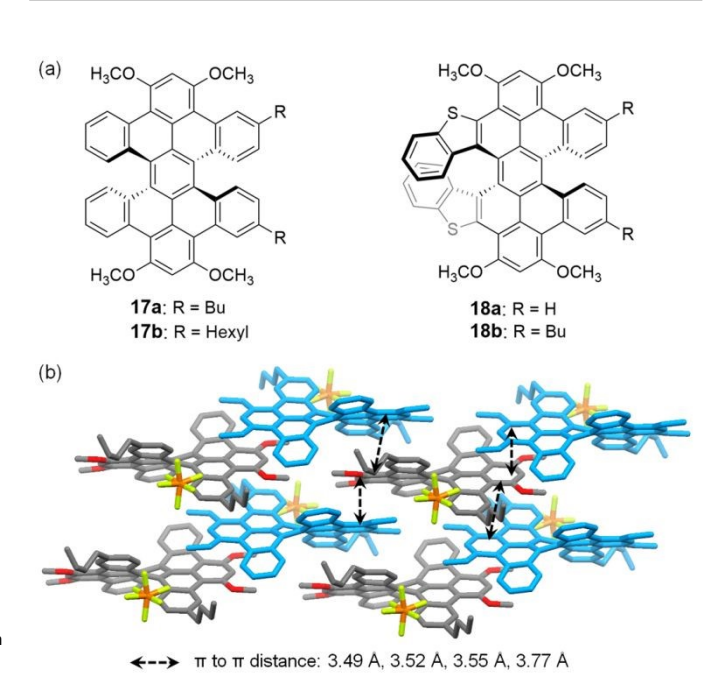


Fig. 6 (a) Double helicenes 17a/b and 18a/b; (b) $\pi-\pi$ stacking in the crystal of $17a^+$ PF₆-, where the (M, M) enantiomer is shown in blue, and the (P, P) enantiomer is colored according to the elements. Reproduced with permission from ref. 40. Copyright 2022 American Chemical Society.

Double helicenes were recently been demonstrated by Miao and coworkers to be an effective structural motif for stabilizing radical cations. Chemical oxidation of double [5]helicene **17a/b** (Fig. 6) yielded a robust radical cation, showing negligible spectral changes after its CH_2Cl_2 solution was exposed to ambient air in the dark for 60 days. ⁴⁰ Such a high stability is attributed to spin delocalization in the π -backbone and the twisted structure impeding dimerization. Notably, crystal structures of neutral **17a** and radical cation salt **17a***+PF₆⁻ exhibit nearly identical π - π stacking, with PF₆-occupying the site of CH_2Cl_2 in the neutral crystal. Dip-coated films of **17a***+PF₆- showed conductivity up to 1.32 ± 0.04 S cm⁻¹,

Open Access Article. Published on 19 2025. Downloaded on 20/11/25 23:15:55.

ARTICLE

Journal Name

while **17a** behaved as a p-type semiconductor with mobility of 0.064 \pm 0.003 cm² V $^{-1}$ s $^{-1}$. Moreover, photochemical oxidation of **17b** in the solid state with O $_2$ generated its radical cation, enabling OFETs to function as nonvolatile optoelectronic memory with switching contrast above 10^3 and long-term stability. Similarly, S-containing double helicenes **18a/b** (Fig. 6) formed robust radical cations. **18a***+ remained stable in CH $_2$ Cl $_2$ under ambient air in the absence of light for four weeks and retained ~85% absorption in water-saturated CH $_2$ Cl $_2$ after 8 days. 41 The salt **18b***+SbF $_6$ - achieved a conductivity of 0.16 S cm $^{-1}$ at room temperature, due to strong $\pi-\pi$ interactions in its crystal structure.

2.2 Nitrogen-containing systems

Stable radical cations often feature heteroatoms that act as spin-bearing sites,⁴² and tertiary arylamines have long been used to develop radical cation species. For example, N,N,N',N'-tetramethyl-*p*-phenylenediamine (Fig. 7), can be readily converted by one-electron oxidation into a stable semiquinone radical, known as Wurster's blue.⁴³ Another example is tris(4-bromophenyl)ammoniumyl hexachloroantimonate, which is commonly known as magic blue (Fig. 7) and used as a popular oxidizing agent in organic and organometallic chemistry.

Fig. 7 Resonance structure of Wurster's blue and structure of magic blue.

Triphenylamine radical cations lacking para substituents are inherently unstable due to high spin densities at para positions. 44 Stabilization can be achieved by ortho-bridging aryl groups, as seen in triarylamines 19-23 (Fig. 8), which enhance planarity of π -frameworks and delocalize spin density. Crystal structures reveal that neutral trioxytriphenylamine 19 is shaped like a shallow bowl with a sp3-hybridized central N atom, whereas its radical cation is flat with shorter C-N bonds. 45 The delocalization of unpaired spin across the π -framework of 19°+, including oxygen atoms, prevents dimerization or oxygenation under ambient conditions. Similarly, the radical cations of S, C, C-bridged triarylamine 20 46 and O, C, C-bridged triarylamines 21a/b ⁴⁷ all exhibited appreciable stability, with the absorption spectra of their CH2Cl2 solutions remaining virtually unchanged after one day and the crystals of their hexachloroantimonate salts being stable under ambient conditions. In the crystals, the π -frameworks of 20°+ and 21a°+ are essentially flat while that of 21b*+ is slightly twisted. DFT calculations indicate spin delocalization across all three radicals, with the highest density on the central nitrogen. Notably, sulfur in 20°+ shares more spin density than oxygen in 21a** and 21b**. Spin density on the central N atom increases in the order of 20^{++} (+0.294) < $21a^{++}$ (+0.328) < $21b^{++}$ (+0.332), while Mulliken charges on it decrease in the order of 20°+ $(+0.345) > 21a^{+} (+0.290) > 21b^{+} (+0.194).$

Very recently, Kivala et al. synthesized trithiatriphenylamine 22a (Fig. 8) and compared it to 22b/c (Fig. 8) WHTH PEWENTHIA bridges. ⁴⁸ The radical cation of **22a**, in the form of **22a***+SbCl₆-, remained stable for months under ambient conditions, showing no degradation in either solid or CH2Cl2 solution. In contrast, 22b*+ and 22c*+ exhibited significantly lower stabilities, with half-lives of 1.06 and 6.04 days, respectively, in tetrachloroethane at 80 °C under inert atmosphere. Spin delocalization differences explain this stability: the spin density of 22a*+ is delocalized across the whole molecule while that of 22b*+ is mostly distributed over the methoxylated phenothiazine subunit and that of 22c*+ is localized on the phenothiazine ring. The crystal structure of 22a°+SbCl6exhibits a planarized π-backbone relative to the saddle-shaped neutral molecule and one-dimensional stacking of 22a*+. Additionally, 22a forms charge-transfer complexes with 7,7,8,8-tetracyanoquinodimethane (TCNQ) or F₄-TCNQ, transferring 0.29 e- and 0.42 e- to TCNQ in the 1:1 and 2:1 complexes, respectively, or 0.90 e- to F₄-TCNQ in the 1:1 complex, as determined from anion bond lengths. In these crystals, molecules of 22a and TCNQ or F4-TCNQ stack in a column with an alternative arrangement. However, the electrical conductivities of these charge transfer complexes as well as **22a***+SbCl₆- were not reported.

Compound **23a**, a sp^3 hybridized carbon-bridged triphenylamine, is oxidized by Ag⁺ to it radical cation, which is isolated in the form of **22a***+(Al(OC(CF₃)₃)₄)⁻ and characterized by X-ray crystallography. ⁴⁹ Similar to **19***+, the polycyclic framework of **23a***+ adopts a planar conformation, in contrast to the shallow bowl-shaped geometry of neutral **23a**. DFT calculations indicate that the central N atom in **23a***+ carries a higher spin density (+0.366) compared to **19***+ (+0.328), indicating greater localization of the unpaired electron. When oxidized with 0.5 equivalent of Ag⁺(Al(OC(CF₃)₃)₄)⁻, **23a** forms a

ARTICLE

Journal Name

dimerized product, suggesting the reactivity of **23a***. Compound **23b**, a sterically protected triphenylamine derivative of **23a**, incorporates spiro-fluorene moieties perpendicular to the planar triphenylamine core and *tert*-butyl groups at para positions. ⁵⁰ Its radical cation remains stable in CH₂Cl₂ solution for months at 7 °C under N₂ and in solid form under ambient conditions for weeks.

Fig.9 Triarylamine-incorporated double helicenes 24-26 and phenylenediamine-linked

Incorporating ortho-bridged triphenylamine into a double helicene structure provides additional kinetic protection for its radical cation through helical curvature around the spin centre, as demonstrated in compounds 24-26 (Fig. 9). The radical cations of 24 and 25 were crystallized as 24°+SbCl6- and 25°+NTf2-, respectively. 51, 52 Crystal structures reveal that oxidation induces planarization in both molecules, accompanied by shortened helical pitches in their radical cation states. Notably, the absorption spectrum of 24°+SbCl₆in CH2Cl2 solution remained unchanged for 2 weeks under ambient air and room light, whereas 25°+NTf2- retained its spectral profile for 1 day under an inert atmosphere. Compound 26, a double hetero[5]helicene synthesized via oxidative dimerization of benzo[b]phenoxazine, 53 forms stable radical cations in both racemic and enantiopure forms with different counteranions, which influence the molecular packing in the resulting radical cation salts. 54 Racemic and enantiopure $26^{\circ +} NTf_2^-$ exhibit one-dimensional π - π stacking with counteranions intercalated between stacks, though enantiomers in the racemic crystal are separated by a larger π - $\boldsymbol{\pi}$ distance. In contrast, in the racemic and enantiopure 26°+SbCl₆- crystals, the interactions between 26°+ and SbCl₆prevent continuous π - π stacking of **26**** likely due to the matching between the curvature of 26°+ and the spherical shape of the $SbCl_6^-$ anion. Despite the close π - π stacking, racemic and enantiopure crystals 26°+NTf2- exhibited low

conductivity of 1.22×10^{-8} S cm⁻¹ and $2.86\times10^{-8}_{\text{N-N}}\text{Scle}_{\text{cm}}^{-1}_{\text{ling}}$ respectively. For comparison, vacuum deposited of the first respectively. The first respectively are seniconductor with a field effect mobility of 2×10^{-5} cm² V⁻¹ s^{-1.53} Incorporating triphenylamine into a larger curved π -scaffold yields phenylenediamine-linked nanographene **27** (Fig. 9) whose radical cation remains stable in CH₂Cl₂ solution for 8 days under ambient conditions without degradation. Interestingly, **27** adopts a Z-shaped *anti* conformation in its neutral state, whereas its radical cation assumes a C-shaped *syn* conformation in the **27**°+SbF₆- crystal. The stability of **27**°+ can be attributed to contribution from quinoidal resonance in **27**°+ and kinetic protection from the curved π -scaffold.

N, N'-disubstituted dihydrodiazaacenes, such as compounds **28a-c** ⁵⁶ (Fig. 10), serve as general π -scaffolds to stabilize radical cations because one-electron oxidation transforms their central dihydropyrazine ring from antiaromatic to nonaromatic or weakly aromatic, as evidenced by DFT-calculated nucleus-independent chemical shift (NICS) values. This stabilization mechanism also applies to the radical cation of compound 28 (Fig. 10).57 Consequently, the radical cations of 28a-c and 29 exhibit comparable stability with their absorption spectra essentially unchanged under ambient conditions for at least 24 h. Crystal structures reveal that the diazaacene backbones of 28a-c are flat in both neutral and radical cations forms, while the dibenzo[a,c]phenazine backbone of 29 changes from a V-shaped conformation in the neutral state to a twisted conformation in the radical cation, with the dihydropyrazine ring flattened. Notably, the formation of stable radical cation of 28a is related to the doping of p-type semiconductors based on N,N'-disubstituted dihydrodiazapentacenes.58,59

Fig. 10 N, N'-disubstituted-dihydrodiazaacenes 28a-c and related structures.

Based on the radical cation of N,N'-disubstituted dihydrophenazine, Wang *et al.* developed a water-soluble bissulfonate salt **30** (Fig. 10).⁶⁰ The radical cation in **30** resists dimerization and disproportionation, attributable to intermolecular Coulombic repulsion and steric hindrance from

Open Access Article. Published on 19 2025. Downloaded on 20/11/25 23:15:55

ARTICLE

sulfonate groups. It also has an appropriate electron density to avoid reactions with oxygen or water. As a result, 30 exhibits remarkable stability, with no decomposition observed in aqueous solution under ambient conditions for more than 70 days (monitored by UV-vis spectroscopy). Aqueous organic redox flow batteries using **30** as the posolyte and ZnCl₂ as the negolyte demonstrated extremely stable performance over 2500 cycles (~27 days). Radical cation 31°+ (Fig. 10), also known as viridium,61 features a structure related to N,N'disubstituted dihydrophenazine. It exhibits exceptional thermodynamic stability in solution under ambient conditions, as confirmed by Electron Paramagnetic Resonance (EPR) and UV-vis spectroscopy over two months, due to full spin delocalization across its π -backbone. In the solid state, 31°+ arranges into one-dimensional columns with a π - π distance of 3.29 Å. In aqueous or perfluorohydrocarbon solutions, it forms π-stacked dimers.

As an electron-rich aromatic heterocycle prone to oxidation, pyrrole serves as a building block for π -conjugated radical cations. While N-annulated rylenes formally incorporate fused pyrrole units, their radical cations are not further discussed here because their spin density and singly occupied molecular orbitals are delocalized across the rylene backbone but located minimally on the nitrogen atoms.⁶² Pyrrole-containing multiple cations are discussed in the next session. N,N'-diarylated tetrabenzotetraaza[8]circulene 32a/b (Fig. 11) yields highly stable radical cations upon chemical oxidation.⁶³ This stability is highlighted by the 83% yield of 32a*+ obtained after aqueous work-up, CH₂Cl₂ extraction, and silica gel column chromatography under ambient conditions. The stability arises spin of density from delocalization across tetrabenzotetraaza[8]circulene backbone, with the highest spin density localized on the α -carbons of the N-octylated pyrrole units. In their hexachloroantimonate salt crystals, 32a** and 32b** both exhibit planar structures but adopt distinct stacking arrangements: 32a*+ forms eclipsed stacking with an intermolecular π – π distance of 3.32 Å, whereas **32b*** adopts a slip-stacked arrangement. Pyrrole-embedded buckybowl 33a and its planar analogue 33b generate radical cations of different reactivities in solution.⁶⁴ Despite similar spin delocalization across the π -backbones with higher spin density localized on pyrrole carbons, the reactivity divergence arises from the strain induced by the positive curvature of 33a. In both single crystals and low temperature solution states, 33a*+ undergoes reversible σ -dimerization between the internal pyrrole α -carbons, whereas **33b**** selectively forms a π -dimer with a short π - π distance of 3.14 Å.

Fig. 11 Pyrrole-embedded molecules 32 and 33.

2.3 Sulfur-containing systems

Sulfur-containing π -conjugated radical cations often feature sulfur atoms in thiophene or tetrathiafulvalene (TTF) units, as exemplified by the molecules shown in Fig. 12a and 11b, respectively. The radical cations of bithiophene terthiophene their are sterically protected in bicyclo[2.2.2]octene-fused derivatives 34 and 35a (Fig. 12a),65 similar to the sterically congested hydrocarbons 5 and 6 (Fig. 2). Such kinetical stabilization allows the crystals of 34°+SbF₆- and 35a**SbF₆- to be stable without decomposition after the crystals were left to stand at room temperature under air for one month. The structure of 35°+ involves a significant contribution from the quinoidal resonance as indicated by crystal structure and ESR measurement as well as theoretical calculations. Notably, oxidation of sterically protected bithiophene and terthiophene (34 and 35) with NO+SbF₆yields radical cations, whereas longer oligothiophenes under the same conditions form dications. Without bicyclo[2.2.2]octene moiety at the centre thiophene ring, **35b**** forms π -dimer with intermolecular distance as short as 2.976 Å between the beta carbon atoms of the central thiophene units. 66 Compound 36 is a macrocycle composed of four ethynylene-thienylene and two vinylene-thienylene units, whose radical cation remains stable in solid state but degrades in CH₂Cl₂ solution under ambient condition.⁶⁷ In the crystal of **36°**+SbF₆⁻, **36°**+ forms a π -dimer, (**35°**+)₂, with intermolecular S...S distances of 3.7-3.8 Å comparable to twice the standard van der Waals radius of sulfur atom. Spin-coated films of 36 from its CS₂ solution exhibited a room temperature conductivity of 5.7×10^{-8} S cm⁻¹, but became a p-type semiconductor after annealing at 100°C, with a lower conductivity of 9.2×10⁻¹¹ S cm⁻¹ and a field effect mobility of 1.4×10⁻⁴ cm² V⁻¹ s⁻¹, suggesting formation of **36***+ in the thin film self-oxidation of **36** in air.⁶⁸

Open Access Article. Published on 19 2025. Downloaded on 20/11/25 23:15:55

ARTICLE Journal Name

Fig. 12 (a) Thiophene-containing molecules; (b) TTF-containing zwitterions.

Tetrathiafulvalene (TTF) is a well-established π -scaffold for stable radical cations, as its five-membered ring becomes aromatic with six π -electrons upon one-electron oxidation. A recent notable example is zwitterion 37 (Fig. 12b), which has a carboxylate anion attached to the $\pi\text{-conjugated}$ radical cation core. It exhibits exceptionally high conductivity: 530 S cm⁻¹ at 300 K and 1,000 S cm⁻¹ at 50 K. ⁶⁹ DFT calculations reveal that the spin density in 37 is localized primarily on the carboxylateconnected TTF unit, balancing the negative charge of the carboxylate with the positive charge of the TTF moiety. Notably, 37 is unique among the radical cations discussed here, as its single-crystal structure has not been reported. Due to lack of single crystals, the high conductivity of 37 was measured from disordered bulk solids rather than crystalline materials. DFT calculations suggest stable dimeric structures in the solid state, featuring anti-parallel arrangements in both face-to-face and side-by-side stacking. Zwitterion 38, with a structure closely related to 37, form hydrogen-bonded organic frameworks (HOFs) in the solid state.⁷⁰ Tuning crystallization conditions yields two polymorphs of 38, which exhibit roomtemperature conductivities of 6.07×10⁻⁷ and 1.35×10⁻⁶ S cm⁻¹, respectively, as measured in pressed pellets of crystalline powder.

3. Multiple radical cations

Conjugated multiple radical cations, which possess more than one unpaired electron and/or carry more than a single positive charge, can in principle be created by incorporating several redox active π -units into a single framework. The structural factors that stabilize monoradical cations, discussed previously, are not reiterated here to avoid redundancy. This approach is exemplified by the diradical dication 392(++), which

results from reduction of cyclobis(paraguat-paphenylene) tetracation (394+),71,72 as shown in Fig. 139. Specifically, 39260 forms an inclusion complex with methyl viologen radical cation (40°+) by three-electron reduction of an equimolar mixture of 39⁴⁺ and 40²⁺. This spontaneous encapsulation of 40°+ inside the cavity of $39^{2(++)}$ arises from favorable radical-radical interactions occurring between the three 4,4'-bipyridinium radical cations. The binding constant of this inclusion complex was determined using isothermal titration calorimetry and UV/vis spectroscopy as $(5.0\pm0.6)\times10^4~M^{-1}$ and $(7.9\pm5.5)\times10^4$ M⁻¹, respectively. Crystal structure shows that the bipyridinium radical cation subunits in 40°+ and 392(°+) are separated by 3.22 Å as measured from their centroids, and quantum chemistry calculations indicate partial charge transfer from the guest (40°+) to the host (392(°++)), with calculated charges of +1.18 and +1.71, respectively. In the crystal of the complex, 39^{2(*+)} arranges into one-dimensional columns with π - π distance of 3.28 Å. These π - π interactions enable the salt of $40^{\circ+}\square 39^{2(\bullet+)}$ $3PF_6^-$ to perform as a p-type semiconductor in a single-crystal field effect transistor with a hole mobility up to 0.05 cm² V⁻¹ s⁻¹. ⁷³ Notably, $39^{2(\bullet+)}$ was also crystallized alone as its hexafluorophosphate salt, where 39²⁽⁺⁺⁾ stacks into a one-dimensional column with an even shorter π - π distance (3.12 Å), highlighting the dominance of strong radicalradical interactions in driving solid-state packing. In addition, the radical-radical interactions of 392(++) have been applied in developing rotaxanes and catenanes.74,75

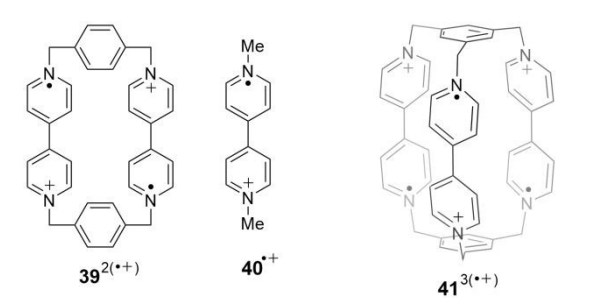


Fig. 13 Macrocyclic multiple radical cations based on 4,4'-bipyridinium.

On the basis of tetracation 394+, Stoddart et al. further developed a hexacationic organic cage, 416+, by incorporating three redox-active building blocks of 4,4'-bipyridinium dications into a triangular prism-shaped symmetry.76 Reduction of 416+ with cobaltocene results in its triradical trication 413(++), which has a doublet ground state. Its quartet state is only 0.08 kcal mol⁻¹ higher in energy than the doublet, suggesting a strong intramolecular exchange coupling. 413(++) was crystallized in the form of CH₃CN\(\Pi\)41^{3(\(\beta\)+)} 3PF₆⁻, where a molecule of CH₃CN occupies the cavity of **41**^{3(•+)}. In the crystal structure, **41**^{3(•+)} arranges into a hexagonal porous superstructure with interconnected one-dimensional channels. Each channel is formed by taking advantage of the strong radical-pairing interactions with a stacking distance of 3.15 Å between the bipyridinium radical cations and the π - π stacking between the phenylene units in the adjacent cages.

Open Access Article. Published on 19 2025. Downloaded on 20/11/25 23:15:55

Journal Name ARTICLE

Fig. 14 Multiple triarylamine-based molecules that afford multiple radical cations.

Incorporating several bridged triarylamines units in one molecule allows formation of multiple radical cations through oxidation. The overall radical nature of the resulting cationic species depends on the interactions between the individual radical sites. Macrocycles 42a/b (Fig. 14) contain S-bridged triphenylamine units connected by methylene groups. 42a³⁽⁺⁺⁾ and 42b4(*+) are formed by oxidation of each S-bridged triphenylamine unit to the radical cation, with spin density delocalized on each planarized phenothiazine unit.⁷⁷ They were both isolated in the form of hexafluoroantimonate salts, and $42a^{3(\bullet+)}$ appeared more stable than $42b^{4(\bullet+)}$, with its characteristic absorption barely changed after 48 h at room temperature. The capability of forming stable radical cations allow 42a and 42b to function as cathode materials in lithiumion batteries with initial discharge capacities of 19.3 mAh g-1 and 28.7 mAh g⁻¹, respectively.

Compound 43a comprises two sulfur and carbon-bridged triphenylamine (SCBT) units linked by a 1,8-naphthalene moiety, while 43b contains two oxygen and carbon-bridged triphenylamine (OCBT) units. Stepwise chemical oxidation of 43a results in the radical cation and diradical dication, which were isolated in the form of 43a*+SbCl₆- and 43a^{2(*+)}2NTf₂-, and both species are stable under ambient conditions.⁷⁸ Singlecrystal X-ray diffraction analyses revealed that both 43a*+ and **43a**^{2(•+)} adopt intramolecular face-to-face close π -stacking of the SCBT units, which arises from covalent-like bonding interactions between the sulfur atoms. This is evidenced by significantly shortened S···S distances of 3.37 Å in 43a*+ and 3.03 Å in 43a²⁽⁺⁺⁾, both well below twice the van der Waals radius of sulfur (3.60 Å). In contrast, the crystal structures of neutral **43b**, **43b***+SbCl₆⁻ and **43b**^{2(•+)}2SbCl₆⁻ reveal that the two OCBT units progressively separate upon oxidation, with no

intramolecular π - π stacking observed in the dicationic state 43b²⁽⁺⁺⁾. In the crystal of 43a*+SbCl₆-, the SCBTP ให้กับรัชส์ดีให้ ให้เป a one-dimensional column, while in of 43a²⁽⁺⁺⁾2NTf₂-, the naphthalene linkers stack into one-dimensional columns, with no intermolecular overlap between SCBT units. Owing to the π - π interactions in the solid state, compressed pellets of **43a***+SbCl₆⁻ and **43a**^{2(*+)}2NTf₂⁻ exhibited room-temperature conductivity of 1.9×10^{-6} S cm⁻¹ and 1.4×10^{-7} S cm⁻¹, respectively. Dication **44**²⁺ has two carbon-bridged triphenylamine units linked through a C-C single bond and was oxidative dimerization by of triphenylamine 23a (Fig. 8). 49 It has an open-shell singlet ground state, with a diradical character of 0.77. The radicals in 44²⁺ interact through resonance as shown in Fig. 14, unlike the radicals in 42a3(++) and 43a2(++). Compound 45 contains two Cbridged triphenylamine units fused with hexa-perihexabenzocoronene.⁷⁹ The dication **45**²⁺ contains small contribution of open-shell singlet, with a diradical character of 0.20, which is in line with the C-N bond is shorter upon oxidation, suggesting the small contribution of diradical dication character. In both 45°+ and 45°+, π - π stacking are

Conjugated macrocycles containing multiple triphenylamine units, such as compounds 46-48 (Fig. 15), enable stable multiple radical cations. Chemical oxidation of compounds 46a and 46b yields stable diradical dication that can be stored under ambient conditions. 80, 81, 82 Having 1,4-phenylene linkers, **46a**^{2(•+)} exhibits a triplet ground state with spins and charges delocalized over two 1,4-phenylenediamine moieties. In contrast, having 9,10-anthrylene linkers, 46b2(++), exhibits a singlet ground state with spins and charges localized on two 1,3-phenylenediamine moieties, supported by shortening of the corresponding C-N bonds. In the solid state, 46a²⁽⁺⁺⁾ arranges into a one-dimensional chain in the crystal structures of $46a^{2(\bullet+)}2SbF_6^-$ and $46a^{2(\bullet+)}2(Al(OC(CF_3)_3)_4)^-$, but not in the crystal structure of $46a^{2(\bullet+)}2(B(C_6F_5)_4)^-$. Macrocycles 47a/b and 48 (Fig. 15) exhibit rich redox properties, with several cationic species isolated and characterized.^{83, 84} 47a²⁺ and 47a⁴⁺ were both isolated as hexachloroantimonate salts. The open-shell singlet ground states of 47a2+ and 47a4+ exhibit diradical characters of 0.862 and 0.379, respectively, with 47a²⁺ being globally aromatic and 47a4+ globally antiaromatic. In contrast, the oxidized species of 47b was isolated as a radical trication. Similarly, chemical oxidation of bismacrocycle 48 generates **48**^{2(•+)}, which possesses an open-shell singlet ground state with a high diradical character of 0.96. Similar redox behavior is observed for their hydrocarbon analogue 49 (Fig. 15).85 492+, isolated in the form of 492+2SbF₆-, exhibits a globally aromatic, open-shell singlet ground state, with multiple diradical characters (y_0 =0.46, y_1 =0.37, y_2 =0.16) calculated from the crystal structure.

Open Access Article. Published on 19 2025. Downloaded on 20/11/25 23:15:55

ARTICLE Journal Name

Fig. 15 Conjugated macrocycles that afford multiple radical cations.

Sessler et al. synthesized cyclo[8]pyrrole in its dicationic form, **50**²⁺SO₄²⁻ (Fig. 15) and subsequently oxidized it to the radical trication 50°3+ using I2.86,87 The side chains in 50°3+ play a crucial role in determining the packing motifs of the radical trications in the resulting crystals. Diffusion of hexane vapor into a dichloromethane solution yielded (50a*3+SO₄²⁻)₂·I₂₅²⁻·I₂, in which $50a^{-3}+SO_4^{2-}$ units form slipped π -dimers without interdimer $\pi\text{-}\pi$ interactions. Using ethyl acetate instead of hexane resulted in $(50a^{-3+}SO_4^{2-})_2 \cdot I_7^- \cdot I_{24}^-$, where two **50a** $^{\circ 3+}$ SO₄ $^{2-}$ units sandwich an I₇ $^{-}$ ion, and these sandwiches are intercalated by layers of 1D polyiodide I₂₄- (Fig. 16a). In the crystal structure of $50b^{-3+}SO_4^{2-}\cdot I_{12}^-$, the $50b^{-3+}SO_4^{2-}$ units are intercalated by 1D polyiodide chains, forming a linear 1D stacked donor-acceptor structure. For 50c*3+SO₄2-·I₁₆-, the 50c*3+SO42- units assemble into 2D highly ordered layers, which are intercalated with 2D polyiodide layers of I₈⁻ and I₂₄⁻,

leading to a linear 1D donor-acceptor cocrystal structure (Fig. 16b). Single-crystal of $(50a^{-3+}SO_4^{2-})_2 \cdot I_7^{-} \cdot I_2 \stackrel{\frown}{l_7} \stackrel{\frown}{l_7} 50b^{-13+} SO_4^{2-5} \stackrel{\frown}{l_1} \stackrel{\frown}{l_2} \stackrel{\frown}{l_7} \stackrel{\frown}{l_7}$ **50c*** $^{3+}$ SO₄ $^{2-}$ ·I₁₆ $^{-}$ exhibited conductivity of 3.6±0.4×10⁻⁴ S cm⁻¹, $7.2\pm0.7\times10^{-3}$ S cm⁻¹ and $6.1\pm0.6\times10^{-1}$ S cm⁻¹, respectively, under ambient temperature. In addition, 50a2+SO42- can transfer electrons to macrocycle 51 via proton-coupled electron transfer (PCET) or through an artificial electron transport chain (ETC) using I2 as mediators and trifluoroacetic acid as proton source. This process generates the radical trication 50a*3+ in the crystal 50a*3+SO42-(CO2CF3)- and the radical dication H₃51°²⁺ in the crystals H₃51°²⁺2(CO₂CF₃)⁻·CHCl₃ or $(H_351^{-2+})_2SO_4^{2-}\cdot 2I_3^{-}\cdot 2.5I_2\cdot 6.25H_2O$.

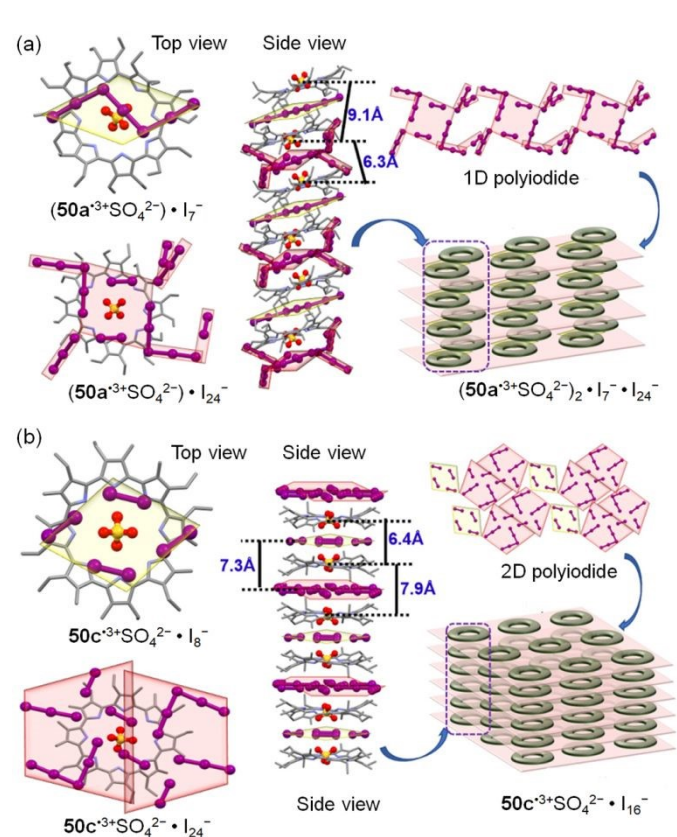


Fig. 16 Crystal structures of $(50a^{*3+}SO_4^{2-})_2 \cdot I_7 - I_{24} - (a)$ and $50c^{*3+}SO_4^{2-} \cdot I_{16} - (b)$ with cartoon representation. Reproduced with permission from ref. 86. Copyright 2025 American Chemical Society.

Other notable examples of multiple radical cations include **52** $^{(2\bullet)+}$, **53** $^{2(\bullet+)}$ and **54** $^{2(\bullet+)}$, as shown in Fig. 17. Azatriangulene diradical monocation 52(2*)+ features a polycyclic framework isoelectronic with the triangulene diradical, where a cationic sp²-hybridized nitrogen atom replaces the central carbon atom of triangulene. Two derivatives, **52**^{(2•)+}, **53**^{2(•+)}, were isolated as **52a** $^{(2\bullet)+}$ SbCl₆⁻ and **52b** $^{(2\bullet)+}$ (SO₃CF₃)⁻, respectively. ^{88, 89} They both have a triplet ground state, analogous to triangulene, with spin density delocalized along the periphery of the azatriangulene backbone. This spin is kinetically stabilized by trichlorophenyl and mesityl substituents. As a result, 52b(2•)+(SO₃CF₃)- exhibits excellent stability, showing no changes in its absorption spectrum after 10 hours or in fluorescent intensity after 5000 seconds. Oxidation of diindinodihydrophenazine 53 with I2 generates its diradical

Open Access Article. Published on 19 2025. Downloaded on 20/11/25 23:15:55

ARTICLE Journal Name

dication as the solid $53^{2(\bullet+)}2I_3^-$, which is benchtop stable for several months under ambient conditions.90 A large excess of reducing reagents and base is required to reduce 53²⁽⁺⁺⁾ back to 53. Di(benzothiino)pyrene 54 can be stepwise oxidized to and **54**^{2(•+)} using 1 or 2 equivalents $NO^{+}(Al(OC(CF_3)_3)_4)^{-.91}$ Upon one-electron oxidation, one 1,4dithiane ring becomes planar, with the spin density primarily localized on this ring and a concomitant contraction of the S-C bond lengths. As a result, $54^{2(\bullet+)}$ adopts a fully planar backbone and possesses a triplet ground state.

52a^{(2*)+}: Ar =
$$\frac{C}{Ar}$$
 CI

Ar

 $\frac{N}{Bu}$
 \frac{N}

4. Fractional radical cations

Fractional radical cations here refer to charged π -systems that, on average, bear non-integer charges and/or unpaired spins. These fractional charges or unpaired spins typically arise from the association of radical cations with neutral molecules in specific stoichiometric ratios, resulting in mixed-valence species. An early example is the mixed-valence salt of naphthalene (naph), reported by Fritz et al. in 1978. 92 In this crystal, the naphthalene radical cation (naph)*+ forms a mixedvalence dimer, (naph)2°+, where the two crystallographically indistinguishable components are arranged in a face-to-face π stack with an interplanar separation (3.2 Å) apparently shorter than the sum of their van der Waals radii. Polycrystalline pellets of $(naph)_2^{\bullet+}PF_6^-$ exhibit a room-temperature conductivity of 0.12 ± 0.046 S cm⁻¹. Mixed-valence salts, exemplified by (naph)₂*+PF₆-, played a pivotal role in the development of organic conductors and superconductors. 93 Besides naphthalene, other polycyclic aromatic hydrocarbons, such as pyrene (pyr), perylene (per), and fluoranthene (flu), form mixed-valence salts through electrocrystallization. 94, 95, 96, ⁹⁷ Single crystals of (pyr)₁₂(AsF₆)₇ exhibits metallic conducting behaviour in 200-300 K, and those of (per)₂(AsF₆)_{1.1}·(CH₂Cl₂)_{0.7} and $(per)_2(AsF_6)_{0.75}(PF_6)_{0.35} \cdot (CH_2Cl_2)_{0.85}$ exhibit very high conductivities of 1200 S cm⁻¹ at 300K and 70000 S cm⁻¹ around 285 K, respectively, owning to the 1D stacks of perylene molecules in the mixed-valence salts. In contrast,

polycrystalline samples of (TP)2PF6, (flu)2PF6 vexhibit olow conductivity of 7 × 10⁻³ S cm⁻¹ and 0.05 ¹\$.1୧ନନ୍¹D5ର ଦେଖି temperature, respectively.98

Fig. 18 Structures of TTF analogues and derivatives.

Tetrathiafulvalene (TTF) not only forms radical cation salts as shown in Fig. 1, but also participates in mixed-valence systems, exemplified by the TTF-TCNQ complex, the first purely organic material reported to exhibit electrical conductivity comparable to that of metals. 99 The high conductivity of TTF-TCNQ arises from its mixed-valence state, in which TTF and TCNQ carry partial charges of +0.59 and -0.59, respectively, and form segregated stacks in the solid state. 100,101 Similarly, TTF analogues and derivatives also support mixed-valence states. A prominent example is tetramethyltetraselenafulvalene (TMTSF, Fig. 17), which forms superconducting mixed-valence salts. (TMTSF)₂•+PF₆- exhibits a conductivity of 10⁵ S cm⁻¹ around 20 K at ambient pressure and was the first organic superconductor discovered, with a superconducting transition temperature of 0.9 K under a pressure of 12 kbar, 102 while single crystals of (TMTSF)2*+ClO4transit to a superconductor below 1.4 K in the absence of applied pressure. 103

Compound 55 (Fig. 18) can be regarded as an indenofluorene-extended tetrathiafulvalene (TTF). Oxidation of 55 via electrocrystallization yields either the mixed-valence salt 55·(BF₄)_{1.5} or the radical cation salts 55°+PF₆- and 55°+TaF₆-, depending on the electrolyte employed. 104 The mixed-valence salt contains 55°+ and 552+ in a 1:1 ratio. In the crystal structures of all three salts, the 55 cations form onedimensional (1D) π -stacks. However, **55**·(BF₄)_{1.5} exhibits a larger π – π distance (3.69 Å) than the other two salts, indicating stronger electrostatic repulsion between 55°+ and **55**²⁺ compared to that between **55***+ ions. As measured from the compressed powdered samples, at room temperature, **55**·(BF₄)_{1.5}, **55**°+PF₆ $^-$ and **55**°+TaF₆ $^-$ exhibit room-temperature conductivities of 1.3×10^{-3} , 3.07×10^{-2} , and 5.32×10^{-2} S cm⁻¹, respectively. All three salts behave as semiconductors, with conductivity decreasing by four to five orders of magnitude upon cooling to 77 K. Consistent with the intrinsic conductivity observed in the radical cation salts of 55, a butylated derivative of 55 functions as a p-type organic semiconductor in single crystals transistors with a field effect mobility of 1.44 cm² V⁻¹ s⁻¹.¹⁰⁵ In contrast to the 1,3-dithiole rings of TTF, anion 56*- (Fig. 18) features two 1,3-thiazole rings connected through conjugated nitrogen atoms and has a radical cation in

Journal Name

ARTICLE

This article is licensed under a Creative Commons Attribution-NonCommercial 3.0 Unported Licence

Open Access Article. Published on 19 2025. Downloaded on 20/11/25 23:15:55.

its π -backbone. Adding tetramethylbenzidine (**57** in Fig. 18) to a solution of **56*** led to the formation of the **56·57** $_2$ complex as blue crystals. Mulliken population analysis indicates an overall charge of -1.6 on **56** and +0.8 on **57**, confirming significant electron transfer from **57** to **56**. The charge-transfer complex of **56·57** $_2$ effectively absorbs across the full solar spectrum, extending beyond 2500 nm, and was therefore employed as a photothermal material, achieving a photothermal conversion efficiency of 49.6%.

Compound 58 (Fig. 19), a derivative of bispyrrole-fused bisanthene, presents a rare example for radical cations exhibiting symmetry-broken intermolecular charge separation in the solid state. 107 Stepwise oxidation of 58 with NO+SbF₆generates **58**°+ and **58**²⁺, distinguishable by absorption spectroscopy. DFT-calculated spin density indicates that spin is largely distributed along the periphery of 58°+. Interestingly, Xray crystallography combined with DFT calculation-based Mulliken population analysis reveals that the crystal of 58°+SbF₆⁻ is in fact a mixed valence complex comprising two different forms of 58: a shallow bowl-shaped form bearing more positive charge (58^{m+}) and an essentially flat form bearing less positive charge (58 $^{n+}$). In the crystal, the two forms of 58 arrange into a π -stack with the repeating sequence of $58^{m+} \cdot \cdot \cdot 58^{n+} \cdot \cdot \cdot 58^{m+}$. Upon increasing the temperature from 173 K to 298 K, the degree of charge transfer decreases, with m decreasing from 1.4 to 1.3 and n increasing from 0.6 to 0.7. This reduced charge transfer is accompanied with a reduced bowl depth and an increased π - π distance between **58** $^{m+}$ and **58** $^{n+}$.

Fig. 19 Polycyclic heteroarenes that form fractional radical cations.

Compounds 59a and 59b (Fig. 19) are O and Scontaining anthanthrenes, which form mixed valence salts, 592 COF and 59b₃(ClO₄)₂, via electrocrystallization. ¹⁰⁸ In the crystals of these mixed valence salts, 59a and 59b molecules form 1D column, with shorter π - π distances (<3.40 Å) and greater π - π overlaps than the corresponding neutral crystals. The single crystals of **59a**₂ClO₄ and **59b**₃(ClO₄)₂ exhibit room temperature conductivities up to 0.11 S cm⁻¹ and 0.031 S cm⁻¹, respectively. In connection with electrical conductivities of these mixed valence salts, compounds 59a and 59b and their derivatives in neutral forms have been applied as p-type organic semiconductors in OFETs. For example, the 3,9-diphenyl derivative of 59a in vacuum-deposited films achieved a field effect mobility of 0.43-0.46 cm² V⁻¹ s⁻¹, and the devices were demonstrated to be stable for five months under ambient conditions. 109

Compounds **60a** and **60b** (Fig. 19) are a pair of regioisomeric polycyclic O-heteroarenes, which form mixed valence salts, and **60b**₃(ClO₄)₂·THF·(H₂O)_{0.5}, **60a**₁₀(PF₆)₆·(THF)₁₆ electrocrystallization. 110 In the crystals, the 60a units assemble into a π-stacked column with an antiparallel arrangement and an average interplanar spacing of 3.33(7) Å, in contrast to the herringbone packing of neutral 60a. Similarly, the 60b units arrange into a π-stacked column with both pincer-like and head-to-tail packing modes and π - π distances varying from 3.21 to 3.42 Å (Fig. 20a) The crystallographically independent molecules of 60a and 60b within each stack display nearly identical bond lengths, indicating effective charge the entire π -column. Two-terminal delocalization across devices fabricated from а single crvstal of 60b₃(ClO₄)₂·THF·(H₂O)_{0.5} exhibited semiconducting behavior, demonstrated by its sigmoidal I-V curves and an increase in conductivity with rising temperature. The room-temperature conductivity reached values of up to 3.7×10⁻³ S cm⁻¹ (ohmic) and 5.1×10^{-3} S cm⁻¹ (non-ohmic).

Benzannulated B,N-doped corannulenes 61a and 61b (Fig. 19) undergo one-electron oxidation with NO+SbF₆- in the presence of NaBArF₄ (ArF = 3,5-bis(trifluoromethyl)phenyl) to mixed-valence salts **61a**₃^{2(•+)}(BAr^F₄⁻)₂ 61b₃^{2(•+)}(BAr^F₄-)₂. These salts exhibit high thermal stabilities under an inert atmosphere and could be stored for several weeks at room temperature. 111 In these crystals, both 61a and **61b** exist as π -stacked trimers, **61a**₃^{2(•+)} and **61b**₃^{2(•+)} (Fig. 20b), with intra-trimer π - π distances of 3.28–3.29 Å and 3.34–3.35 Å, respectively. These π -stacked trimers further stack to form a column with intertrimer distances of 3.50 Å for 61a and 3.50 Å for 61b. EPR spectroscopy and DFT calculations indicate that 61a₃^{2(•+)} and 61b₃^{2(•+)} possess an open-shell singlet ground state, with the majority of the unpaired electrons located on the B-N bonds. As measured from the compressed pellets under a pressure of 3 MPa, 61a₃^{2(•+)} and 61b₃^{2(•+)} exhibit low conductivity of 2.48×10^{-7} S cm⁻¹ and 3.44×10^{-7} S cm⁻¹, respectively.

Journal Name ARTICLE

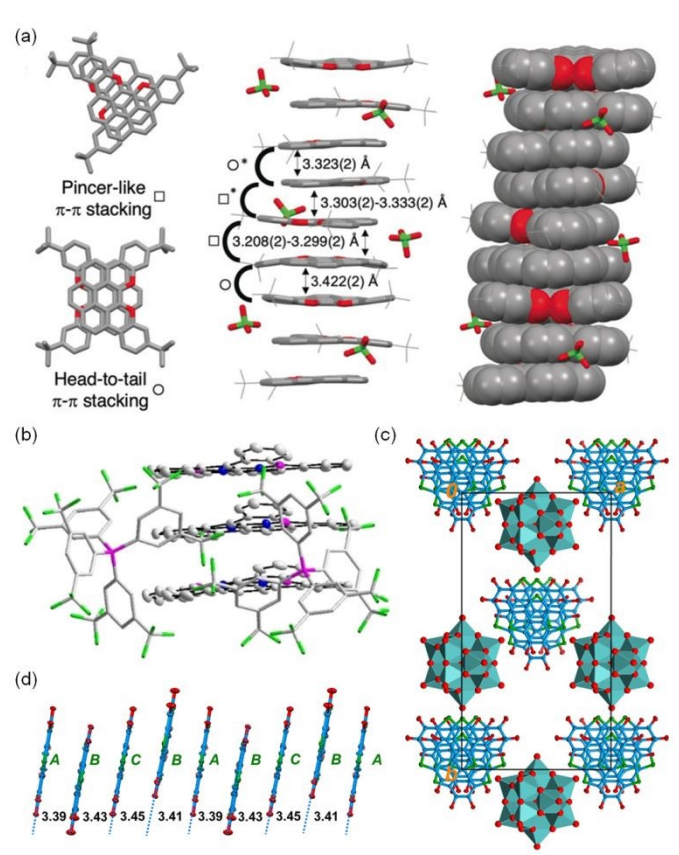


Fig. 20 (a) π - π stacking in the crystal structure of **60b**₃(ClO₄)₂·THF·(H₂O)_{0.5}; (b) π -stacked trimer in the crystal structure of **61b**₃²⁽⁺⁺⁾(BAF^F₄-)₂; (c) a unit cell in the crystal structure of **62a**₄³⁺(PMO₁₂O₄₀)³⁻; (d) π - π stacking in the crystal structure of **62a**₄³⁺(PMO₁₂O₄₀)³⁻. Reproduced with permission from ref. 110–112. Copyright 2020, 2023 and 2024 Wilev.

Trithiasumanene 62a and triselenasumanene 62b (Fig. 19) form four mixed-valence salts via electrocrystallization: **62a**₅³⁺(BAr^F₄⁻)₃, **62b**₅³⁺(BAr^F₄⁻)₃, **62a**₄³⁺(PMo₁₂O₄₀)³⁻ $62b_4^{3+}(PMo_{12}O_{40})^{3-}$ (Ar^F = 3,5-bis(trifluoromethyl)phenyl).¹¹² In the BArF4- salts, the BArF4- anions organize into hexagonal channels that accommodate 1D π -stacked columns of $62a_5^{3+}$ or $62b_5^{3+}$. The crystal structure of $62a_5^{3+}(BAr^F_4^-)_3$ contains 10 crystallographically independent 62a molecules, each adopting a shallow bowl-shaped conformation with bowl depths ranging from 0.51 to 0.73 Å and Mulliken charges varying from +0.24 to +1.10. These units pack in a convex-concave arrangement with an average π - π distance of 3.52 Å. The crystal structure of **62b**₅³⁺(BAr^F₄⁻)₃ contains 5 crystallographically independent molecules of 62b, which are all nearly flat and have Mulliken charges varying from +0.41 to +1.0. In the crystal structure of $62a_4^{3+}(PMo_{12}O_{40})^{3-}$ (Fig. 20c), three crystallographically independent 62a molecules (labeled A, B, and C in Fig. 20d) adopt a flat π -framework with Mulliken charges of +0.99, +0.65, and +0.71, respectively. They assemble into π -stacked columns with a repeating ···A-B-C-B··· pattern and an average interplanar distance of 3.42 Å. Temperature-dependent electrical conductivity, measured on single crystals using a four-probe method, indicates that all four salts behave as semiconductors with thermally activated conductivity. 62b₄3+(PMo₁₂O₄₀)3- exhibit room temperature conductivity of 3.5×10⁻³ S cm⁻¹, while other three mixed-valence salts exhibit conductivity around $1.5\times10^{-4}~{\rm S}~{\rm cm}^{-1}$. The venductivity observed in the mixed-valence salt of **62B**9s the p-type semiconductor behavior exhibited by a butylated derivative of **62b** in single-crystal transistors, which achieves a field-effect mobility of $0.37~{\rm cm}^2~{\rm V}^{-1}~{\rm s}^{-1}.^{113}$

5. Conclusions and outlook

The exploration of robust, fully characterized π -conjugated radical cations reveals a clear evolutionary path in their stabilization and application. While early strategies relied heavily on steric protection to isolate radical cations of simple polycyclic arenes, this approach often comes at the cost of electronic communication in the solid state, limiting its utility for functional materials. A more powerful paradigm has emerged through the use of π -units, such as phenalenyl, flattened triarylamines, and TTF, which confer thermodynamic stability by efficiently delocalizing spin and charge. This fundamental insight has been pivotal, enabling the development of organic conductors and semiconductors with conductivity without sacrificing intermolecular interactions. The recent identification of promising new motifs, such as double (hetero)helicenes and conjugated macrocycles, further enriches this toolkit for intrinsic stabilization.

In p-type organic semiconductors, the neutral molecule represents the undoped state, enabling high on-off ratios in OFETs, while the radical cations (including mixed-valence states) constitute the doped, higher-conductivity state. However, studies on the neutral and radical cation forms of the same π -system are often conducted in isolation. Only a handful of systems, such as TMTP (Fig. 1), 17a (Fig. 6), and 59a (Fig. 19), have been investigated in both states, typically using field-effect transistors for the neutral form and twoterminal devices for the radical cation. Bridging these largely separate research domains is a promising direction for future research. π -systems proven in conductive radical cation salts could inspire design of new high-mobility semiconductors for OFETs. Simultaneously, robust radical cations from highmobility neutral semiconductors offer a direct pathway to novel, highly conductive organic materials. A concerted effort to explore both states of the same molecular core will provide deeper insights into organic semiconductor design and accelerate the development of new materials.

Conflicts of interest

There are no conflicts to declare.

Data availability

No primary research results have been included, and no new data were generated or analyzed as a part of this review article.

Acknowledgements

ARTICLE Journal Name

This research was supported by the Research Grants Council of Hong Kong (CRF C4001-23G) and the State Key Laboratory of Synthetic Chemistry.

Notes and references

- N. L. Bauld, Radicals, Ion Radicals, and Triplets, Wiley-VCH, New York, 1997, 141.
- Y. Shirota and H. Kageyama, Chem. Rev., 2007, 107, 953-
- F. Wudl, G. M. Smith and E. J. Hufnagel, J. Chem. Soc. D, 1970, 1453-1454.
- F. Wudl, D. Wobschall and E. J. Hufnagel, J. Am. Chem. Soc., 1972, 94, 670-672.
- H. Urayama, H. Yamochi, G. Saito, K. Nozawa, T. Sugano, M. Kinoshita, S. Sato, K. Oshima, A. Kawamoto and J. Tanaka, Chem. Lett., 1988, 17, 55-58.
- B. Dhara, M. Nakamura, K. Bulgarevich, K. Takimiya Cryst. Growth Des. 2024, 24, 5826-5833
- G. Heywang and S. Roth, Angew. Chem. Int. Ed. Engl., 1991, 30, 176-177.
- K. Takimiya, K. Bulgarevich, M. Abbas, S. Horiuchi, T. Ogaki, K. Kawabata and A. Ablat, Adv. Mater., 2021, 33, e2102914
- U. Geiser and J. A. Schlueter, Chem. Rev., 2004, 104, 5203-5242.
- 10 T. Sugawara, H. Komatsu and K. Suzuki, Chem. Soc. Rev., 2011, 40, 3105-3118.
- Z. Mi, P. Yang, R. Wang, J. Unruangsri, W. Yang, C. Wang and J. Guo, J. Am. Chem. Soc., 2019, 141, 14433-14442.
- M. Imran, C. M. Wehrmann and M. S. Chen, J. Am. Chem. Soc., 2020, **142**, 38-43.
- Z. X. Chen, Y. Li and F. Huang, Chem, 2021, 7, 288-332.
- D. Yuan, W. Liu and X. Zhu, Chem, 2021, 7, 333-357.
- S. Dong and Z. Li, J. Mater. Chem. C, 2022, 10, 2431-2449.
- 16 L. Ji, J. Shi, J. Wei, T. Yu and W. Huang, Adv. Mater., 2020, 32, e1908015.
- Q. Peng, A. Obolda, M. Zhang and F. Li, Angew. Chem. Int. *Ed.*, 2015, **54**, 7091-7095.
- W. Zeng and J. Wu, Chem, 2021, 7, 358-386.
- B. Tang, J. Zhao, J. F. Xu and X. Zhang, Chem. Sci., 2020, 11, 1192-1204.
- Z. Cui, A. Abdurahman, X. Ai and F. Li, CCS Chem., 2020, 2, 1129-1145.
- F. Tani, M. Narita and T. Murafuji, ChemPlusChem, 2020, 85, 2093-2104.
- T. Harimoto and Y. Ishigaki, ChemPlusChem, 2022, 87, e202200013.
- W. Wang, P. Sun, X. Liu, X. Zhang, L. Zhang, Y. Z. Tan and X. Wang, Org. Lett., 2024, 26, 1017-1021.
- P. T. Herwig, V. Enkelmann, O. Schmelz and K. Müllen, Chem. Eur. J., 2000, 6, 1834-1839.
- M. Banerjee, S. V. Lindeman and R. Rathore, J. Am. Chem. Soc., 2007, 129, 8070-8071.
- J. Guo, C. Zhou, S. Xie, S. Luo, T. Y. Gopalakrishna, Z. Sun, J. Jouha, J. Wu and Z. Zeng, Chem. Mater., 2020, 32, 5927-5936.
- H. Hayashi, J. E. Barker, A. Cardenas Valdivia, R. Kishi, S. N. MacMillan, C. J. Gomez-Garcia, H. Miyauchi, Y. Nakamura, M. Nakano, S. I. Kato, M. M. Haley and J. Casado, J. Am. Chem. Soc., 2020, 142, 20444-20455.
- T. Nishinaga, K. Komatsu, N. Sugita, H. J. Lindner and J. Richter, J. Am. Chem. Soc., 1991, 115, 11642-11643.
- P. L. Magueres, S. V. Lindeman and J. K. Kochi, Org. Lett., 2000, 2, 3567-3570.
- T. Horibe, S. Ohmura and K. Ishihara, J. Am. Chem. Soc.,

- View Article Online 2019, **141**, 1877-1881. DOI: 10.1039/D5SC06726J
- Y. Zhang, S. H. Pun and Q. Miao, Chem. Rev., 2022, 122, 14554-14593.
- T. Kubo, Y. Goto, M. Uruichi, K. Yakushi, M. Nakano, A. 32 Fuyuhiro, Y. Morita and K. Nakasuji, Chem. Asian J., 2007, 2, 1370-1379.
- C. M. Wehrmann, R. T. Charlton and M. S. Chen, J. Am. Chem. Soc., 2019, 141, 3240-3248.
- G. Xie, V. Brosius, J. Han, F. Rominger, A. Dreuw, J. Freudenberg and U. H. F. Bunz, Chem. Eur. J., 2020, 26, 160-164.
- C. Sato, S. Suzuki, K. Okada and M. Kozaki, Chem. Asian J., 2018, **13**, 3729-3736.
- M. Harada, M. Tanioka, A. Muranaka, T. Aoyama, S. Kamino and M. Uchiyama, Chem. Commun., 2020, 56, 9565-9568.
- Y. K. Loh, P. Vasko, C. McManus, A. Heilmann, W. K. Myers, S. Aldridge, Nat. Commun. 2021, 12, 7052.
- M. Narita, T. Teraoka, T. Murafuji, Y. Shiota, K. Yoshizawa, S. Mori, H. Uno, S. Kanegawa, O. Sato, K. Goto and F. Tani, Bull. Chem. Soc. Jpn., 2019, 92, 1867-1873.
- C. Zhu, K. Shoyama and F. Wurthner, Angew. Chem. Int. Ed., 2020, 59, 21505-21509.
- Y. Wang, Q. Gong, S. H. Pun, H. K. Lee, Y. Zhou, J. Xu and Q. Miao, J. Am. Chem. Soc., 2022, 144, 16612-16619.
- L. Zhang, M. Gao, S. Su, Z. Zhou, H. K. Lee, X. Chen, Z. Huang and Q. Miao, Chem. Eur. J., 2025, 31, e202501062.
- A. Ito, Y. Ono and K. Tanaka, Angew. Chem. Int. Ed., 2000, 39, 1072-1075
- C. Wurster and E. Schobig, Ber. Dtsch. Chem. Ges., 1879, 12, 1807-1813.
- E. T. Seo, R. F. Nelson, J. M. Fritsch, L. S. Marcoux, D. W. Leedy and R. N. Adams, J. Am. Chem. Soc., 1966, 88, 3498-3503.
- M. Kuratsu, M. Kozaki and K. Okada, Angew. Chem. Int. Ed., 2005, 44, 4056-4058.
- S. I. Kato, T. Matsuoka, S. Suzuki, M. S. Asano, T. Yoshihara, S. Tobita, T. Matsumoto and C. Kitamura, Org. Lett., 2020, 22, 734-738.
- S. Kataoka, S. Suzuki, Y. Shiota, K. Yoshizawa, T. Matsumoto, M. S. Asano, T. Yoshihara, C. Kitamura and S. I. Kato, J. Org. Chem., 2021, 86, 12559-12568.
- J. Borstelmann, V. Gensch, D. Fehn, M. E. Miehlich, F. Hampel, F. Rominger, K. Meyer and M. Kivala, Angew. Chem. Int. Ed., 2025, 64, e202423802.
- X. Zheng, X. Wang, Y. Qiu, Y. Li, C. Zhou, Y. Sui, Y. Li, J. Ma and X. Wang, J. Am. Chem. Soc., 2013, 135, 14912-14915.
- T. A. Schaub, T. Mekelburg, P. O. Dral, M. Miehlich, F. Hampel, K. Meyer and M. Kivala, Chem. Eur. J., 2020, 26, 3264-3269.
- D. Sakamaki, D. Kumano, E. Yashima and S. Seki, Chem. Commun., 2015, 51, 17237-17240.
- K. Harada, C. Hasegawa, T. Matsumoto, H. Sugishita, C. Kitamura, S. Higashibayashi, M. Hasegawa, S. Suzuki and S. I. Kato, Chem. Commun., 2023, 59, 1301-1304.
- D. Sakamaki, S. Tanaka, K. Tanaka, M. Takino, M. Gon, K. Tanaka, T. Hirose, D. Hirobe, H. M. Yamamoto and H. Fujiwara, J. Phys. Chem. Lett., 2021, 12, 9283-9292.
- D. Sakamaki, H. Sekiguchi, S. Suzuki and H. Fujiwara, Chem. Eur. J., 2025, **31**, e202500942.
- L. Ruan, R. Li, M. Li, Y. Huang and P. An, J. Org. Chem., 2025, 90, 4365-4373.
- G. Xie, N. M. Bojanowski, V. Brosius, T. Wiesner, F. Rominger, J. Freudenberg and U. H. F. Bunz, Chem. Eur. J., 2021, **27**, 1976-1980.
- B. Huang, H. Kang, X.-L. Zhao, H.-B. Yang and X. Shi, Cryst. Growth Des., 2022, 22, 3587-3593.
- X. Gu, B. Shan, Z. He and Q. Miao, ChemPlusChem, 2017, 82,

2025. Downloaded on 20/11/25 23:15:55.

Journal Name ARTICLE

1034-1038

- 59 L. Zhang, Y. Zhao, J. Li, Y. Fu, B. Peng, J. Yang, X. Lu and Q. Miao, J. Am. Chem. Soc., 2025, 147, 3459-3467.
- 60 L. Li, Y. Su, Y. Ji and P. Wang, J. Am. Chem. Soc., 2023, 145, 5778-5785.
- 61 H.-P. J. de Rouville, C. Gourlaouen, D. Bardelang, N. Le Breton, J. S. Ward, L. Ruhlmann, J. M. Vincent, D. Jardel, K. Rissanen, J. L. Clement, S. Choua and V. Heitz, *J. Am. Chem. Soc.*, 2025, **147**, 1823-1830.
- 62 Q. Qi, P. M. Burrezo, H. Phan, T. S. Herng, T. Y. Gopalakrishna, W. Zeng, J. Ding, J. Casado and J. Wu, *Chem. Eur. J.*, 2017, **23**, 7595-7606.
- 63 Y. Matsuo, T. Tanaka and A. Osuka, Chem. Eur. J., 2020, 26, 8144-8152.
- 64 H. Yokoi, S. Hiroto and H. Shinokubo, J. Am. Chem. Soc., 2018, 140, 4649-4655.
- T. Nishinaga, A. Wakamiya, D. Yamazaki and K. Komatsu, J. Am. Chem. Soc., 2004, 126, 3163-3174.
- 66 D. Yamazaki, T. Nishinaga, N. Tanino and K. Komatsu, J. Am. Chem. Soc., 2006, 128, 14470-14471.
- 67 T. Fujiwara, A. Muranaka, T. Nishinaga, S. Aoyagi, N. Kobayashi, M. Uchiyama, H. Otani and M. Iyoda, *J. Am. Chem. Soc.*, 2020, **142**, 5933-5937.
- T. Fujiwara, M. Takashika, M. Hasegawa, Y. Ie, Y. Aso, S. Aoyagi, H. Otani and M. Iyoda, ChemPlusChem, 2019, 84, 694-703.
- Y. Kobayashi, T. Terauchi, S. Sumi and Y. Matsushita, *Nat. Mater.*, 2017, 16, 109-114.
- 70 M. Vicent-Morales, M. Esteve-Rochina, J. Calbo, E. Orti, I. J. Vitorica-Yrezabal and G. Minguez Espallargas, J. Am. Chem. Soc., 2022, 144, 9074-9082.
- 71 A. Trabolsi, N. Khashab, A. C. Fahrenbach, D. C. Friedman, M. T. Colvin, K. K. Coti, D. Benitez, E. Tkatchouk, J. C. Olsen, M. E. Belowich, R. Carmielli, H. A. Khatib, W. A. Goddard III, M. R. Wasielewski and J. F. Stoddart, *Nat. Chem.*, 2010, 2, 42-49.
- 72 A. C. Fahrenbach, J. C. Barnes, D. A. Lanfranchi, H. Li, A. Coskun, J. J. Gassensmith, Z. Liu, D. Benitez, A. Trabolsi, W. A. Goddard III, M. Elhabiri and J. F. Stoddart, J. Am. Chem. Soc., 2012, 134, 3061-3072.
- 73 A. C. Fahrenbach, S. Sampath, D. J. Late, J. C. Barnes, S. L. Kleinman, N. Valley, K. J. Hartlieb, Z. Liu, V. P. Dravid, G. C. Schatz, R. P. Van Duyne and J. F. Stoddart, ACS Nano, 2012, 6, 9964-9971.
- 74 Y. Jiao, Y. Qiu, L. Zhang, W. G. Liu, H. Mao, H. Chen, Y. Feng, K. Cai, D. Shen, B. Song, X. Y. Chen, X. Li, X. Zhao, R. M. Young, C. L. Stern, M. R. Wasielewski, R. D. *Nature*, 2022, 603, 265-270.
- 75 Y. Jiao, H. Mao, Y. Qiu, G. Wu, H. Chen, L. Zhang, H. Han, X. Li, X. Zhao, C. Tang, X. Y. Chen, Y. Feng, C. L. Stern, M. R. Wasielewski and J. F. Stoddart, J. Am. Chem. Soc., 2022, 144, 23168-23178.
- 76 H. Han, Y. Huang, C. Tang, Y. Liu, M. D. Krzyaniak, B. Song, X. Li, G. Wu, Y. Wu, R. Zhang, Y. Jiao, X. Zhao, X. Y. Chen, H. Wu, C. L. Stern, Y. Ma, Y. Qiu, M. R. Wasielewski and J. F. Stoddart, J. Am. Chem. Soc., 2023, 145, 18402-18413.
- 77 L. Mao, M. Zhou, T. Wu, D. Ma, G. Dai and X. Shi, *Org. Lett.*, 2024, **26**, 7244-7248.
- 78 H. Morishita, K. Sambe, S. Dekura, H. Sugishita, C. Kitamura, T. Matsumoto, T. Takeda, R. Uesugi, T. Ishida, T. Akutagawa, S. Suzuki and S. I. Kato, Chem. Eur. J., 2025, 31, e202500576.
- J. Borstelmann, S. Zank, M. Krug, G. Berger, N. Frohlich, G. Glotz, F. Gnannt, L. Schneider, F. Rominger, F. Deschler, T. Clark, G. Gescheidt, D. M. Guldi and M. Kivala, Angew. Chem. Int. Ed., 2025, 64, e202423516.
- R. Kurata, D. Sakamaki and A. Ito, Org. Lett., 2017, 19, 3115-3118.

- 81 W. Wang, L. Wang, S. Chen, W. Yang, ZoZhang and XoWang,
- Sci. China Chem., 2017, 61, 300-305.W. Wang, C. Chen, C. Shu, S. Rajca, X. Wang and A. Rajca, J.
- Am. Chem. Soc., 2018, **140**, 7820-7826.
- 83 S. Dong, T. Y. Gopalakrishna, Y. Han and C. Chi, *Angew. Chem. Int. Ed.*, 2019, **58**, 11742-11746.
- 84 Y. Ma, Y. Han, X. Hou, S. Wu and C. Chi, *Angew. Chem. Int. Ed.*, 2024, **63**, e202407990.
- 85 Z. Li, X. Hou, Y. Han, W. Fan, Y. Ni, Q. Zhou, J. Zhu, S. Wu, K. W. Huang and J. Wu, *Angew. Chem. Int. Ed.*, 2022, **61**, e202210697.
- 86 Y. D. Yang, M. Leng, Q. Zhang, X. Jin, C. V. Chau, J. Yang, S. Vasylevskyi, G. Henkelman, H. Y. Gong, L. Fang and J. L. Sessler, J. Am. Chem. Soc., 2025, 147, 19364-19371.
- 87 Y. D. Yang, Q. Zhang, L. Khrouz, C. V. Chau, J. Yang, Y. Wang, C. Bucher, G. Henkelman, H. Y. Gong and J. L. Sessler, ACS Cent. Sci., 2024, 10, 1148-1155.
- 88 H. Wei, X. Hou, T. Xu, Y. Zou, G. Li, S. Wu, Y. Geng and J. Wu, Angew. Chem. Int. Ed., 2022, 61, e202210386.
- 89 S. Arikawa, A. Shimizu, D. Shiomi, K. Sato, T. Takui, H. Sotome, H. Miyasaka, M. Murai, S. Yamaguchi and R. Shintani, *Angew. Chem. Int. Ed.*, 2023, **62**, e202302714.
- M. Ahmed, Y. Wu, M. R. Schiavone, K. Lang, L. You, M. Zeller and J. Mei, *Org. Lett.*, 2023, 25, 6363-6367.
- 91 S. Tang, L. Zhang, H. Ruan, Y. Zhao and X. Wang, *J. Am. Chem. Soc.*, 2020, **142**, 7340-7344.
- 92 H. P. Fritz, H. Gebauer, P. Friedrich, P. Ecker, R. Artes and U. Schubert, Z. Naturforsch., B: Chem. Sci., 1978, **33**, 498-506.
- 93 G. Saito and T. Murata, Phil. Trans. R. Soc. A., 2008, 366, 139-150.
- 94 A. Schätzle, J. U. Von SchÜTz, H. C. Wolf, H. Schäfer and H. W. Helberg, *Mol. Cryst. Liq. Cryst.*, 1985, **120**, 229-232.
- 95 H. J. Keller, D. Nöthe, H. Pritzkow, D. Wehe, M. Werner, P. Koch and D. Schweitzer, Mol. Cryst. Liq. Cryst., 1980, 62, 181-199.
- 96 P. Koch, D. Schweitzer, R. H. Harms, H. J. Keller, H. Schäfer, H. W. Helberg, R. Wilckens, H. P. Geserich and W. Ruppel, Mol. Cryst. Liq. Cryst., 1982, 86, 87-101.
- 97 H. Endres, H. J. Keller, B. Müller and D. Schweitzer, *Acta Crystallogr., Sect. C: Cryst. Struct. Commun.*, 1985, **41**, 607-613.
- 98 C. Kröhnke, V. Enkelmann and G. Wegner, *Angew. Chem. Int. Ed. Engl.*, 1980, **19**, 912-919.
- 99 J. Ferraris, D. O. Cowan, V. Walatka and J. H. Perlstein, J. Am. Chem. Soc., 1973, 95, 948-949.
- 100 R. Comès, S. M. Shapiro, G. Shirane, A. F. Garito and A. J. Heeger, *Phys. Rev. Lett.*, 1975, **35**, 1518-1521.
- 101 T. E. Phillips, T. J. Kistenmacher, J. P. Ferraris and D. O. Cowan, J. Chem. Soc., Chem. Commun., 1973, 471-472.
- 102 D. Jérome, A. Mazaud, M. Ribault and K. Bechgaard, *J. Physique Lett.*, 1980, **41**, 95-98.
- 103 K. Bechgaard, K. Carneiro, M. Olsen, F. B. Rasmussen and C. S. Jacobsen, *Phys. Rev. Lett.*, 1981, **46**, 852-855.
- 104 M. A. Christensen, C. R. Parker, T. J. Sørensen, S. de Graaf, T. J. Morsing, T. Brock-Nannestad, J. Bendix, M. M. Haley, P. Rapta, A. Danilov, S. Kubatkin, O. Hammerich and M. B. Nielsen, J. Mater. Chem. C, 2014, 2, 10428-10438.
- 105 L. Feng, H. Dong, Q. Li, W. Zhu, G. Qiu, S. Ding, Y. Li, M. A. Christensen, C. R. Parker, Z. Wei, M. B. Nielsen and W. Hu, Sci. China Mater., 2016, 60, 75-82.
- 106 J. Xu, Q. Chen, S. Li, J. Shen, P. Keoingthong, L. Zhang, Z. Yin, X. Cai, Z. Chen and W. Tan, *Angew. Chem. Int. Ed.*, 2022, **61**, e202202571.
- 107 G. Liu, L. Gao, Y. Han, Y. Xiao, B. Du, J. Gong, J. Hu, F. Zhang, H. Meng, X. Li, X. Shi, Z. Sun, J. Wang, G. Dai, C. Chi and Q. Wang, Angew. Chem. Int. Ed., 2023, 62, e202301348.
- 108 O. Matuszewska, T. Battisti, R. R. Ferreira, N. Biot, N.

View Article Online

DOI: 10.1039/D5SC06726J

Shemical Science Accepted Manuscript

ARTICLE Journal Name

Demitri, C. Meziere, M. Allain, M. Salle, S. Manas-Valero, E. Coronado, E. Fresta, R. D. Costa and D. Bonifazi, *Chem. Eur. J.*, 2023, **29**, e202203115.

- 109 N. Kobayashi, M. Sasaki and K. Nomoto, *Chem. Mater.*, 2009, **21**, 552-556.
- 110 L. Ethordevic, C. Valentini, N. Demitri, C. Meziere, M. Allain, M. Salle, A. Folli, D. Murphy, S. Manas-Valero, E. Coronado and D. Bonifazi, *Angew. Chem. Int. Ed.*, 2020, **59**, 4106-4114.
- 111 Y. Gao, Z. Liu, T. Li and W. Zhao, *Angew. Chem. Int. Ed.*, 2023, **62**, e202314006.
- 112 L. Wu, Y. Li, X. Hua, L. Ye, C. Yuan, Z. Liu, H. L. Zhang and X. Shao, *Angew. Chem. Int. Ed.*, 2024, **63**, e202319587.
- 113 B. Fu, X. Hou, C. Wang, Y. Wang, X. Zhang, R. Li, X. Shao and W. Hu, *Chem. Commun.*, 2017, **53**, 11407-11409.

Robust π-Conjugated Radical Cations

View Article Online DOI: 10.1039/D5SC06726J

Shilong Su,^a Qian Miao*, a, b

Department of Chemistry, The Chinese University of Hong Kong, Shatin, New Territories,

Hong Kong, China

b State Key Laboratory of Synthetic Chemistry, The Chinese University of Hong Kong, Shatin, New Territories, Hong Kong, China

* miaoqian@cuhk.edu.hk

Data availability statements

No primary research results, software or code have been included and no new data were generated or analysed as part of this review.